CHIN. PHYS. LETT. Vol. 38, No. 6 (2021) 068103

High-Performance Visible Light Photodetector Based on BiSeI Single Crystal

Xiu Yan(严秀)[1,2], Wei-Li Zhen(甄伟立)[1], Hui-Jie Hu(胡慧杰)[1], Li Pi(皮雳)[1,2], Chang-Jin Zhang(张昌锦)[1,3], and Wen-Ka Zhu(朱文卡)[1*]

[1]*High Magnetic Field Laboratory, Hefei Institutes of Physical Science, Chinese Academy of Sciences, Hefei 230031, China*

[2]*University of Science and Technology of China, Hefei 230026, China*

[3]*Institutes of Physical Science and Information Technology, Anhui University, Hefei 230601, China*

(Received 20 February 2021; accepted 30 March 2021; published online 25 May 2021)

The continuing demand for new optoelectronic devices drives researchers to seek new materials suitable for photodetector applications. Recently, ternary compound semiconductors have entered researchers' field of vision, among which chalcohalides have attracted special interest because of their rich properties and unique crystal structure consisting of atom chains and inter-chain van der Waals gaps. We have synthesized high-quality BiSeI single crystals with [110]-plane orientation and fabricated a photodetector. The optoelectronic measurements show a pronounced photocurrent signal with outstanding technical parameters, namely high responsivity (3.2 A/W), specific detectivity (7×10^{10} Jones) and external quantum efficiency (622%) for $\lambda = 635$ nm, $V_{ds} = 0.1$ V and $P_{opt} = 0.23\,\mathrm{mW/cm^2}$. The high performance of BiSeI photodetector and its layer structure make it a promising candidate for low-dimensional optoelectronic applications.

DOI: 10.1088/0256-307X/38/6/068103

Photodetectors, possessing the ability to transform light into electrical signals, are essential elements used in video imaging, optical communications, biomedical imaging, security, night vision, gas sensing, motion detection and single-photon detection.[1,2] The continuing demand for new optoelectronic devices drives researchers to seek new materials suitable for photodetector applications. Previous efforts were mainly focused on elementary and binary compound semiconductors.[2,3] Recently, ternary compound semiconductors (and even perovskites and organic polymerics) have entered researchers' field of vision, some of which exhibit superior electronic and optoelectronic performance.[4–7] Among ternary materials, chalcohalides $A^{V}B^{VI}C^{VII}$ (A = Sb, Bi; B = S, Se, Te; C = Cl, Br, I) have attracted special interest because of their rich properties such as ferroelectricity,[8] piezoelectricity,[9] thermoelectricity[10,11] and photoconductivity.[12–16] These compounds crystallize in an orthorhombic structure composed of atom chains. It is generally believed that the atoms in the chain are connected by strong bonds, while the inter-chain bonds are relatively weak, i.e., the van der Waals (vdW) interactions. This type of crystal structure usually shows a needle-like morphology and a high degree of anisotropy.[17]

Intensive studies have unveiled the basic properties of these compounds. Chepur *et al.* measured the reflectivity of BiSeBr and BiSeI and determined their semiconductor gaps to be 1.54 eV and 1.32 eV, respectively.[13] Teng *et al.* analyzed the symmetrical coordinates of BiSeI using group theory.[18] On the basis, the infrared and Raman spectra of BiSeI were experimentally investigated.[19] The optical properties of BiSeI, including optical dielectric function, optical constants, absorption, reflectivity and electron energy loss spectra were studied by a spectroscopic ellipsometry technique.[20] Recently, BiSeI single crystal has been identified as an n-type semiconductor with anisotropic resistivity.[21] In addition, BiSeI has also been viewed as a promising photovoltaic material.[14–16,22]

As described above, one of the fundamental characteristics of BiSeI crystals that has not been studied is optoelectronic property. Hence, the purpose of the present work is to investigate the optoelectronic performance of a photodetector fabricated on BiSeI single crystal. Moreover, previous crystal growth techniques to synthesize BiSeI single crystal need to be improved. Due to the inherent growth rate anisotropy, only needle-like morphology is found to be dominant, which hinders the possibility of growing large single crystals. In this work, we have improved the method

Supported by the National Key Research and Development Program of China (Grant No. 2016YFA0300404), the National Natural Science Foundation of China (Grant No. 11874363, 11974356, and U1932216), and the Collaborative Innovation Program of Hefei Science Center, CAS (Grant No. 2019HSC-CIP002).

*Corresponding author. Email: wkzhu@hmfl.ac.cn

© 2021 Chinese Physical Society and IOP Publishing Ltd

to grow BiSeI single crystals. Based on the obtained high-quality single crystal, an optoelectronic device was prepared and tested under a 635 nm laser tuned to various power density. A pronounced optoelectronic signal was observed with outstanding technical parameters, namely high responsivity (3.2 A/W), specific detectivity (7×10^{10} Jones) and external quantum efficiency (622%). The high performance of BiSeI photodetector and its layered structure make it a promising candidate for low-dimensional optoelectronic applications.

Single crystals of BiSeI were grown by a physical vapor transport (PVT) method via two steps.[21] First, polycrystalline BiSeI was synthesized by directly alloying high-purity bismuth, selenium and iodine elements in an evacuated quartz ampoule which was pumped down to 10^{-5} Pa. Raw materials of 5 g were weighed in a ratio of Bi:Se:I = 1:1:1.03, with 3% excess of iodine to complement for the deficiency due to its lower boiling temperature.[23] Then, the sealed ampoule was put into a tube furnace that was in sequence heated up to 600 ℃ in 24 h, held for 12 h, cooled down to room temperature, heated up to 400 ℃ in 24 h, and held for another 24 h. In the second step, the polycrystalline BiSeI was placed horizontally in a double-zone tube furnace to grow single crystals by the PVT method. Prior to single crystal growth, the temperature (T_2) of the growth zone (where single crystals were obtained) was set at 50–100 K higher than the temperature (T_1) of the source zone (where polycrystalline BiSeI was located). It took 24 h for the reversal transport to eliminate possible sediments generated from the previous synthesis procedure. After that, T_1 was adjusted to a higher temperature which was 15 K higher than T_2, to facilitate the evaporation and transport of the source materials and form BiSeI single crystals. This process lasted for a week.

The phase purity of BiSeI crystals was checked by single crystal x-ray diffraction (XRD) on a Rigaku-TTR3 x-ray diffractometer using Cu K_α radiation. The composition and morphology were characterized on a Hitachi TM3000 scanning electron microscope (SEM) equipped with an Oxford energy dispersive spectroscope (EDS) manipulated at 15 kV. Raman spectroscopy was performed on a confocal Raman spectrometer (T64000, Horiba Jobin Yvon) with excitation wavelengths of 532 nm and 633 nm. For the optoelectronic measurements, Au wires were directly connected to the sample using silver paste. The measurements were taken at room temperature using a homemade system composed of a microscope, a four-probe stage, a semiconductor parameter analyzer (2636B, Keithley) and a laser light source with different laser illumination and incident light power density. The laser spot size (about 15 mm in diameter) is much larger than the device's channel area, to ensure uniform illumination. Theoretical investigation of the electronic structures of bulk BiSeI was performed by first principles calculations using the WIEN2k code.[24] The generalized gradient approximation (GGA) of Perdew–Burke–Ernzerhof[25] was employed with a k-mesh of 1000 points. The lattice constants taken from the web site of Springer Materials were adopted for the calculations.

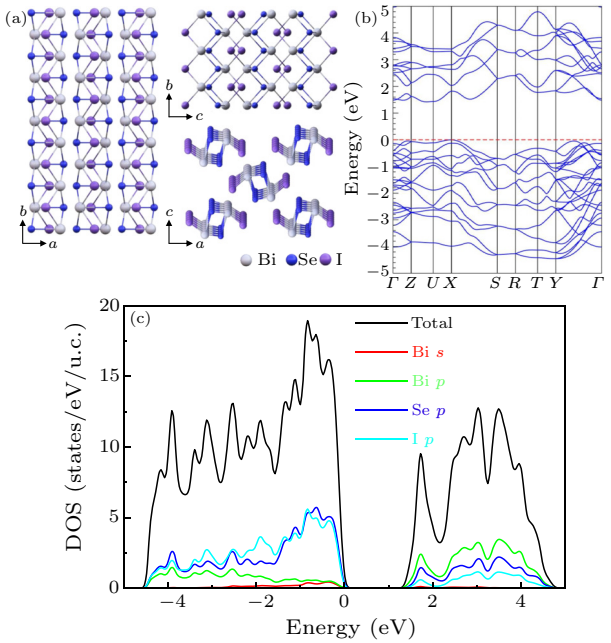

Fig. 1. (a) Schematic crystal structure of BiSeI. Grey, blue and purple spheres represent Bi, Se and I atoms, respectively. (b) Band structures along high symmetry points in the reciprocal space. (c) Total and partial density of states for BiSeI. The Fermi energy is set at the valence band maximum.

A schematic of the crystal structure of BiSeI is shown in Fig. 1(a). It has an orthorhombic symmetry with space group *pnma* (62). The crystal structure is composed of double chains $[(BiSeI)_\infty]_2$ aligned along the b axis, where Bi and Se atoms are connected by covalent bonds and I ions have ionic bonds with a covalent binding bridge (BiSe).[26] The interactions between double chains are weak vdW-type force, making it strongly quasi-one-dimensional (quasi-1D) and anisotropic. Figures 1(b) and 1(c) present the band structures along high symmetry directions and density of states (DOS) for BiSeI, respectively. The calculated band gap is about 1.37 eV, indicating that it is a semiconductor. The calculated value is close to the experimental ones, i.e., 1.29 eV determined by the absorption spectrum[21] and 1.32 eV obtained from the reflectivity measurement,[20] confirming the reliability of our calculations. According to the band structures, the gap is an indirect one as the valence band maximum (VBM) and the conduction band minimum

(CBM) do not appear at the same point. It seems that the VBM is located at point X and the CBM is at the UZ segment. From the DOS plots of BiSeI, the CBM and VBM are mainly composed of distorted p orbitals of Bi, Se and I ions, confirming the nature of covalent bonding.

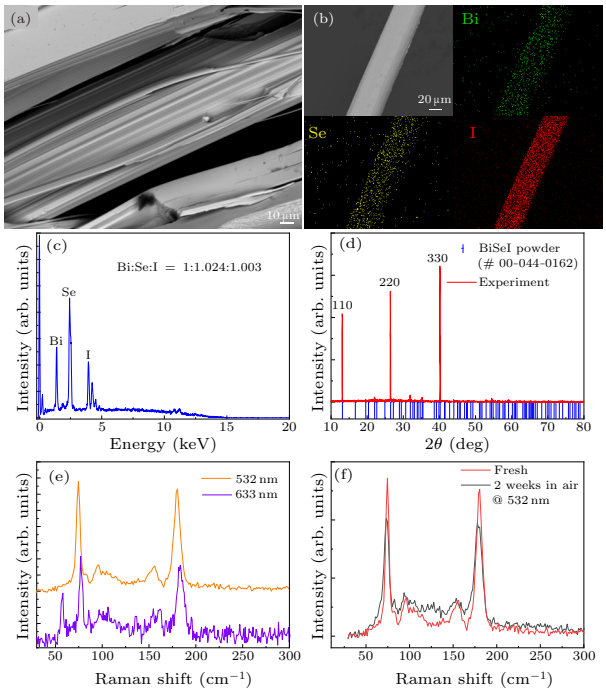

Fig. 2. (a) SEM image of BiSeI showing layered texture. (b) EDS mapping results for the total, Bi, Se and I ionic componential scanning taken on a needle-like crystal. (c) EDS collected at a selected area to reveal the atomic ratio. (d) Single crystal XRD pattern of BiSeI. (e) Raman spectra for BiSeI acquired at room temperature with excitation wavelengths of 532 nm and 633 nm. (f) Raman spectra taken on a sample when freshly cleaved and put in air for two weeks, respectively.

Typical morphology of the as-grown BiSeI single crystal and the element distributions of Bi, Se and I are characterized by SEM and EDS, respectively, as shown in Figs. 2(a)–2(c). The as-grown BiSeI is needle-like crystal with smooth surface and metallic luster, consistent with its quasi-1D crystal structure. Nevertheless, the SEM image taken from the side still shows a feature of layered structure [Fig. 2(a)], suggesting the possibility of exfoliation. Figure 2(b) presents the EDS mapping results for the total, Bi, Se and I ionic componential scanning, confirming the homogeneous distribution of Bi, Se and I atoms. The EDS collected at a selected area indicates that the chemical composition is Bi:Se:I = 1:1.024:1.003 [Fig. 2(c)], which is very close to the stoichiometric ratio. In Fig. 1(d), the XRD pattern shows exclusively one array of diffraction peaks that highly coincide with the [110] diffractions of XRD data of BiSeI powder (PDF No. 00–044-0162),[21] again confirming that our sample is a good single crystal.

Raman spectroscopy provides information about molecular vibrations and is thus a powerful tool for sample identification. Figure 2(e) shows the Raman spectra for the crystal acquired at room temperature with excitation wavelengths of 532 nm and 633 nm, respectively. The slight difference in Raman spectra for different excitation wavelengths is probably due to selective resonance enhancement controlled by electron-phonon coupling. The peaks at lower wave numbers are assigned to the modes of Bi–I bonds and the ones at higher wave numbers are assigned to the Bi–Se modes. Raman bands below 200 cm^{-1} are halogen sensitive and are attributed to modes involving the motion of halogen atoms.[27] In the spectrum excited by the 633 nm laser, the prominent peak at 183 cm^{-1} is obvious evidence of the Bi–Se bond interaction. The appearance of this peak clearly shows the harmonic association when the two components are closer in the crystal without a clear dividing line between each other. The low wave number dispersion of the Bi–Se mode indicates that the interaction between the Bi–Se bond and the adjacent sites in the crystal lattice is negligible. This is consistent with the inter-chain vdW gap mentioned above. These results are in agreement with previous reports both theoretically and experimentally.[18,19] Furthermore, in order to confirm the stability of BiSeI single crystal in air, we remeasured the Raman spectrum after two weeks. In Fig. 2(f), the initial Raman characteristic peaks are almost coincident with those taken in two weeks, which indicates ambient stability of BiSeI single crystal. In one word, the as-grown crystals are high-quality BiSeI single crystal, in terms of the combination of chemical component, structure and Raman vibration characterizations.

To explore the optoelectronic performance of BiSeI, we fabricated a two-terminal device based on BiSeI single crystal. Figure 3(a) shows a schematic illustration of optoelectronic measurement. For the spectral response, different wavelength laser sources were utilized to produce photoresponse with the same intensity of 1.5 mW/cm^2. Figure 3(b) presents responsivity under illumination of different wavelengths ranging from 405 nm to 830 nm. A significant response is obtained in the entire spectrum of interest, which indicates that the BiSeI photodetector can provide broadband photodetection. The time-resolved photoresponse of BiSeI single crystal photodetector under the 635 nm and 0.5 Hz laser is shown in Fig. 3(c). By turning on/off the laser, reversible conversion between high current and low current can be achieved. After several cycles, the current signal exhibits only a slight deviation, which indicates that the detector is stable and repeatable.

We further investigate the incident power density dependence of the photoresponse under illumination of 635 nm laser tuned to various power density. The current-voltage characteristic curves (I–V) for different power density (0–102 mW/cm^2) are plotted in Fig. 3(d). The good linearity demonstrates an Ohmic contact between silver paste and sample. Figure 3(e) shows the I–t switching curve tuned by different laser power density. Distinct optoelectronic response is observed and the photocurrent shows a monotonic dependence upon the laser power density. Figure 3(f) presents the dependence of photocurrent on the laser power density. The dependence can be represented by a power law $I_{\rm ph} \propto P_{\rm opt}^{\theta}$, where $I_{\rm ph}$ is photocurrent, $P_{\rm opt}$ is incident laser power density, and θ is an experimental fitting parameter that usually demonstrates the quality of photoconductivity process. The extracted θ is 0.42, a value close to those previously documented for some photodetectors, e.g., WS_2,[28] GeS,[29] and $PdSe_2$.[30] Such a laser power dependence may be attributed to the trap states that are caused by the defects and/or charged impurities present in the sample.[31] Upon increasing the laser intensity, more traps would be filled by photo-induced charge carriers, leading to the final saturation of photocurrent.

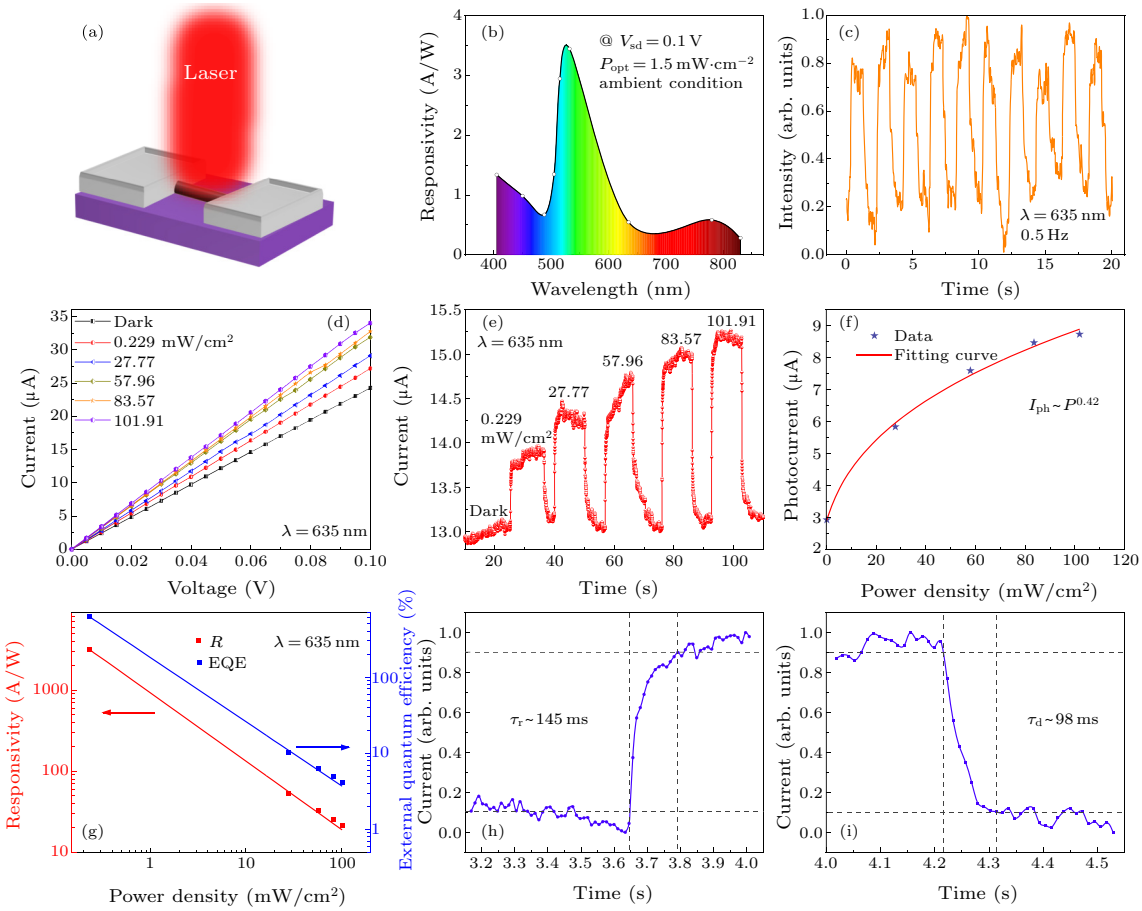

Fig. 3. (a) Schematic illustration of optoelectronic measurement on BiSeI single crystal photodetector. (b) Responsivity as a function of wavelength ranging from 405 nm to 830 nm. (c) Time-resolved photoresponse under 635 nm laser with a frequency of 0.5 Hz. (d) Current-voltage characteristic curves (I–V) taken in darkness and under the 635 nm laser tuned to different laser power density. (e) I–t switching curve tuned by different laser power density. (f) Laser power density dependence of photocurrent. Red line is a fit to the power law. (g) Responsivity and external quantum efficiency as a function of incident power density. (h) Rising time and (i) decaying time recorded at $\lambda = 635$ nm and $V_{\rm ds} = 0.1$ V. Dashed lines are calculation guide.

Some important parameters can be extracted from the data to evaluate the performance of BiSeI photodetector, including response time, responsivity (R), specific detectivity (D^*) and external quantum efficiency (EQE). The device was tested under 635 nm laser with $V_{\rm ds} = 0.1$ V and $P_{\rm opt} = 0.23$ mW/cm^2. Response time reflects the speed of photodetectors to follow a light intensity variation. Upon increasing illumination, the current increases sharply and saturates. As shown in Figs. 3(h) and 3(i), dashed lines are guidelines to calculate rising time $\tau_{\rm r}$ and decaying time $\tau_{\rm d}$ that are defined as the total time needed for the photocurrent to rise from 10% to 90% and decay from 90% to 10% of the peak. The calculated $\tau_{\rm r}$ and $\tau_{\rm d}$

are 145 ms and 98 ms, respectively. Typically, the response time of a photodetector is mainly composed of the photo-induced carrier generation time, transport time and the external circuit time constant.[32] Therefore, improving the carrier mobility is an effective way to further decrease the response time for our device. On the other hand, the relatively slow response may be due to existence of defects, which could be improved by annealing or interfacial modification.

Responsivity is the ratio of the photocurrent to the incident power density, representing the conversion efficiency from the incident light signal with a certain illumination intensity to the electrical signal. Specific detectivity characterizes the detection capability for the lowest optical signal and is designed to compare detectors with different geometries. The external quantum efficiency is defined as the number of detected electrons per incident photon. These parameters can be calculated using the following equations:[33]

$$R = \frac{I_{\rm ph}}{P_{\rm opt} \times S},$$
$$D^* = R\sqrt{\frac{S}{2e\, I_{\rm dark}}},$$
$$\mathrm{EQE} = \frac{hc}{e\lambda}R = \frac{R \times 1240}{\lambda} \times 100\%,$$

where S is the illuminated effective area of the device, e is the electron charge, $I_{\rm dark}$ is the dark current, h is Planck's constant, c is the light velocity in vacuum, and λ is the laser wavelength. All of the measurements were conducted with $V_{\rm ds} = 0.1$ V.

Figure 3(g) shows the responsivity and external quantum efficiency versus incident power density. Different from the dependence of photocurrent, both R and EQE decrease with the increasing incident power density, owing to the absorbance saturation attained by the photodetector and intensified recombination activity at higher light intensity.[34,35] The plotted responsivity as a function of incident power density could be described by the Hornbeck–Haynes model as follows:[36–39]

$$I_{\rm ph} = e\,\eta\Big(\frac{\tau_0}{\tau_{\rm tr}}\Big)\frac{F}{1+(F/F_0)^n},$$

where η is the charge carrier photo-generation quantum efficiency, F is the photon absorption rate, F_0 is the photon absorption rate when the trap states saturation occurs, and n is a phenomenological fitting parameter. The first factor of $(\frac{\tau_0}{\tau_{\rm tr}})$ on the right-hand side is the usual expression for the photoconductive gain, while the second factor $[\frac{F}{1+(F/F_0)^n}]$ accounts for trap saturation at high excitation intensities. At higher illumination intensity the number of available electron traps is decreased. With the traps filled, the number of free electrons increases and the probability of electron-hole recombination is enhanced, leading to reduction in overall responsivity. The maximum responsivity is 3.2 A/W for $P_{\rm opt} = 0.23\,\mathrm{mW/cm^2}$. Correspondingly, the calculated specific detectivity and external quantum efficiency reach as high as 7×10^{10} Jones and 622%, respectively. That is, these parameters are good enough, especially when considering the bias voltage as low as 0.1 V. The performance of BiSeI as a visible light photodetector can be compared to the benchmark materials listed in Table 1, highlighting that BiSeI is a prominent and promising layered semiconductor for more useful electronic and optoelectronic applications.

Table 1. Photoelectric performance comparison of this work with other photodetectors.

Material	Dimension	λ (nm)	R (mA/W)	D^* (Jones)	Response time	References
MoS_2	Monolayer	561	880		4/9 s	[40]
MoS_2	Monolayer	670	7.5		50/50 ms	[41]
WS_2	Monolayer	532	18.8		60/150 ms	[28]
$MnPSe_3$	Nanosheet	375	392.78	2.19×10^9		[42]
PbS	Nanosheet	532	119000		330/350 ms	[43]
PbI_2	bulk	450	180	3.23×10^{11}	323/520 μs	[44]
$CH_3NH_3PbI_3$	bulk	808	240		71/112 μs	[45]
Bi_2Se_3	bulk		2.45		5.32/9.54 s	[46]
BiSeI	bulk	635	3200	7×10^{10}	145/98 ms	this work

In summary, we have synthesized high-quality BiSeI single crystals with [110]-plane orientation and fabricated a photodetector. The optoelectronic measurements show a pronounced photocurrent signal with outstanding technical parameters, namely high responsivity (3.2 A/W), specific detectivity (7×10^{10} Jones) and external quantum efficiency (622%) for $\lambda = 635$ nm, $V_{\rm ds} = 0.1$ V and $P_{\rm opt} = 0.23\,\mathrm{mW/cm^2}$. The high performance of BiSeI photodetector and the layered structure make it a promising candidate for low-dimensional optoelectronic applications.

References

[1] Wang J, Han J, Chen X and Wang X 2019 *Infomat* **1** 33
[2] Luo W *et al.* 2018 *Nano Lett.* **18** 5439

[3] Long M, Wang P, Fang H and Hu W 2019 *Adv. Funct. Mater.* **29** 1803807
[4] Weng S *et al.* 2020 *Phys. Status Solidi Rapid Res. Lett.* **14** 2000085
[5] Li C *et al.* 2020 *Light Sci. & Appl.* **9** 31
[6] Zhu T, Yang Y, Zheng L, Liu L, Becker M L and Gong X 2020 *Adv. Funct. Mater.* **30** 1909487
[7] Li Y, Wang X, Li G, Wu Y, Pan Y, Xu Y, Chen J and Lei W 2020 *Chin. Phys. Lett.* **37** 018101
[8] Fatuzzo E, Nitsche R, Harbeke G, Ruppel W, Roetschi H and Merz W J 1962 *Phys. Rev.* **127** 2036
[9] Berlincourt D, Nitsche R, Merz W J and Jaffe H 1964 *Appl. Phys. Lett.* **4** 61
[10] Rosenthal T, Doeblinger M, Wagatha P, Gold C, Scheidt E W, Scherer W and Oeckler O 2011 *Z. Anorg. Und Allg. Chem.* **637** 2239
[11] Xin J Z, Fu C G, Shi W J, Li G W, Auffermann G, Qi Y P, Zhu T J, Zhao X B and Felser C 2018 *Rare Met.* **37** 274
[12] Sasaki Y 1965 *Jpn. J. Appl. Phys.* **4** 614
[13] Chepur D V, Bercha D M, Turyanitsa I D and Slivka V Y 1968 *Phys. Status Solidi* **30** 461
[14] Kunioku H, Higashi M and Abe R 2016 *Sci. Rep.* **6** 32664
[15] Ganose A M, Butler K T, Walsh A and Scanlon D O 2016 *J. Mater. Chem. A* **4** 2060
[16] Shi H, Ming W and Du M 2016 *Phys. Rev. B* **93** 104108
[17] Arivuoli D, Gnanam F D and Ramasamy P 1987 *J. Mater. Sci.* **22** 981
[18] Teng M K, Balkanski M, Massot M and Ziolkiewicz M K 1974 *Phys. Status Solidi B Basic Solid State Phys.* **62** 173
[19] Kanchana G and Arivuoli D 2001 *Indian J. Eng. & Mater. Sci.* **8** 373
[20] Audzijonis A, Gaigalas G, Zigas L, Sereika R, Zaltauskas R, Balnionis D and Reza A 2009 *Phys. Status Solidi B Basic Solid State Phys.* **246** 1702
[21] Xiao B, Zhu M, Ji L, Zhang B, Dong J, Yu J, Sun Q, Jie W and Xu Y 2019 *J. Cryst. Growth* **517** 7
[22] Ganose A M, Matsumoto S, Buckeridge J and Scanlon D O 2018 *Chem. Mater.* **30** 3827
[23] Yaws C L 1995 in *Handbook of Vapor Pressure*, edited by C. L. Yaws (Gulf Professional Publishing), p 1
[24] Blaha P, Schwarz K, Sorantin P and Trickey S B 1990 *Comput. Phys. Commun.* **59** 399
[25] Perdew J P, Burke K and Ernzerhof M 1996 *Phys. Rev. Lett.* **77** 3865
[26] Fong C Y, Perlov C and Wooten F 1982 *J. Phys. C* **15** 2605
[27] Davies J E D 1973 *J. Inorg. & Nucl. Chem.* **35** 1531
[28] Lan C, Li C, Yin Y and Liu Y 2015 *Nanoscale* **7** 5974
[29] Ulaganathan R K *et al.* 2016 *Nanoscale* **8** 2284
[30] Xu W *et al.* 2020 *Nano Res.* **13** 2091
[31] Ghatak S, Pal A N and Ghosh A 2011 *ACS Nano* **5** 7707
[32] George G and Krusius J P 1994 *J. Lightwave Technol.* **12** 1387
[33] Sun Z and Chang H 2014 *ACS Nano* **8** 4133
[34] Luo P, Zhuge F, Wang F, Lian L, Liu K, Zhang J and Zhai T 2019 *ACS Nano* **13** 9028
[35] Lv L, Zhuge F, Xie F, Xiong X, Zhang Q, Zhang N, Huang Y and Zhai T 2019 *Nat. Commun.* **10** 3331
[36] Guo Q *et al.* 2016 *Nano Lett.* **16** 4648
[37] Long M *et al.* 2020 *Appl. Phys. Lett.* **117** 231104
[38] Soci C, Zhang A, Xiang B, Dayeh S A, Aplin D P R, Park J, Bao X Y, Lo Y H and Wang D 2007 *Nano Lett.* **7** 1003
[39] Schubert M C, Riepe S, Bermejo S and Warta W 2006 *J. Appl. Phys.* **99** 114908 114908
[40] Sanchez O L, Lembke D, Kayci M, Radenovic A and Kis A 2013 *Nat. Nanotechnol.* **8** 497
[41] Yin Z *et al.* 2012 *ACS Nano* **6** 74
[42] Han X *et al.* 2021 *ACS Appl. Mater. & Interfaces* **13** 2836
[43] Gu Y, Wang Y, Xia J and Meng X 2020 *Chin. Phys. Lett.* **37** 048101
[44] Wei Q, Shen B, Chen Y, Xu B, Xia Y, Yin J and Liu Z 2017 *Mater. Lett.* **193** 101
[45] Ding J, Fang H, Lian Z, Li J, Lv Q, Wang L, Sun J and Yan Q 2016 *Crystengcomm* **18** 4405
[46] Zang C, Qi X, Ren L, Hao G, Liu Y, Li J and Zhong J 2014 *Appl. Surf. Sci.* **316** 341